# Wall slip in primitive chain network simulations of shear startup of entangled polymers and its effect on the shear stress undershoot

Yuichi Masubuchi, Dimitris Vlassopoulos, Giovanni Ianniruberto, et al.

Citation: Journal of Rheology **65**, 213 (2021); doi: 10.1122/8.0000194
View online: https://doi.org/10.1122/8.0000194
View Table of Contents: https://sor.scitation.org/toc/jor/65/2
Published by the The Society of Rheology

# Wall slip in primitive chain network simulations of shear startup of entangled polymers and its effect on the shear stress undershoot

Yuichi Masubuchi,[1,a)] Dimitris Vlassopoulos,[2,3] Giovanni Ianniruberto,[4] and Giuseppe Marrucci[4]

[1]*Department of Materials Physics, Nagoya University, Nagoya 4648603, Japan*
[2]*Institute of Electronic Structure and Laser, FORTH, 71110 Heraklion, Crete, Greece*
[3]*Department of Materials Science, Technology, University of Crete, 71003 Heraklion, Crete, Greece*
[4]*Dipartimento di Ingegneria Chimica, dei Materiali e della Produzione Industriale, Università degli Studi di Napoli "Federico II," Piazzale Tecchio, 80-80125 Napoli, Italy*

(Received 20 November 2020; final revision received 18 January 2021; published 19 February 2021)

**Abstract**

In some recent experiments on entangled polymers of stress growth in the startup of fast shear flows, an undershoot in the shear stress is observed following the overshoot, i.e., before approaching the steady state. Whereas tumbling of the entangled chain was proposed to be at its origin, here, we investigate another possible cause for the stress undershoot, i.e., slippage at the interface between the polymer and solid wall. To this end, we extend the primitive chain network model to include slip at the interface between entangled polymeric liquids and solid walls with grafted polymers. We determine the slip velocity at the wall, and the shear rate in the bulk, by imposing that the shear stress in the bulk polymers is equal to that resulting from the polymers grafted at the wall. After confirming that the predicted results for the steady state are reasonable, we examine the transient behavior. The simulations confirm that slippage weakens the magnitude of the stress overshoot, as reported earlier. The undershoot is also weakened, or even disappears, because of a reduced coherence in molecular tumbling. Disentanglement of grafted chains from bulk ones, taking place throughout the stress overshoot region, does not contribute to the stress undershoot.  https://doi.org/10.1122/8.0000194

## I. INTRODUCTION

As it has been known for a long time, entangled polymers exhibit shear thinning, i.e., at sufficiently large shear stresses, the steady-state viscosity decreases with increasing shear rate [1–3]. It is also well known that during the startup of fast shear flows, the transient shear stress shows an overshoot before reaching the steady state [4–6]. Birefringence measurements [5] and molecular simulations [7–9] revealed that the primary molecular mechanism of the overshoot is the flow-induced orientation of entangled subchains between consecutive entanglements [10]. Chain stretch further contributes to the overshoot when the shear rate exceeds the reciprocal Rouse time. Following such well-known overshoot, an undershoot has been observed in some cases [11–14]. Because the undershoot only appears at high shear rates, its origin might be found in either slip at the wall, or edge fracture, or other instabilities, and not necessarily in some molecular mechanisms. Possibly because of such uncertainties, the undershoot has not been frequently discussed in the literature. Recently, however, rheometry developments allow for more reliable measurements at high shear rates [11,12], and a focus on the undershoot now appears appropriate.

Costanzo *et al.* [11] attributed the undershoot to the tumbling motion of the entangled polymer chains under shear, such unexpected tumbling having been revealed by recent molecular simulations of Khomami and co-workers [15–17]. The effect of the tumbling motion is mathematically described by a damped sinusoidal function. Indeed, a fast shear startup initially triggers a coherent tumbling of all molecules, but subsequently, such coherence decays exponentially. The model reasonably reproduces the stress undershoot for some polystyrene melts and solutions [11]. Masubuchi *et al.* [18] run multichain sliplink simulations, confirming the initial coherence of tumbling under the startup of fast shear. Stephanou *et al.* [19] proposed a different molecular theory (the so-called tumbling-snake model), in which the undershoot is also attributed to molecular tumbling.

On the other hand, the undershoot could be linked to other phenomena, such as wall slip [20,21], or even periodic slippage (stick-slip [22–25]), although in those investigations, there is no indication of the existence of a damped periodic response. To examine the effect of transient slippage on the stress growth under shear, Pearson and Petrie [26] proposed a retarded slip boundary condition, in which they introduced the slip relaxation time, reflecting the dependence of slip on the stress history at the wall. Kazatchkov and Hatzikiriakos [27] extended this idea to a multimode memory function. Using a K-BKZ constitutive equation, they reproduced the transient viscosity under slippage conditions quantitatively and determined the relaxation times for the slip dynamics of a commercial linear low-density polyethylene melt from LAOS experiments. Ebrahimi *et al.* [28] used another K-BKZ constitutive model to reproduce the data of a high-density polyethylene melt. However, a single slippage

[a)]Author to whom correspondence should be addressed; electronic mail: mas@mp.pse.nagoya-u.ac.jp

relaxation time was used and chosen to be close to the peak time of the overshoot. In parallel to the constitutive modeling, a stochastic approach was also used by Hatzikiriakos and Kalogerakis [29], who developed a network model to calculate the configuration distribution function resulting from the creation and destruction of transient bonds between the bulk and the wall. They demonstrated that the slippage reduces the magnitude of the stress overshoot, as well as that of the steady-state viscosity.

Though there are no theories and/or simulations linking the undershoot to stick-slip or complete slippage, one might envisage that a transient stick-slip induces a stress undershoot during the stress decrease from the overshoot, i.e., during the approach to the steady state. Indeed, for the case of entangled polybutadiene melts (which are known to be prone to slip because of the large plateau modulus), Dao and Archer [23] observed that at the highest shear rates used the transient shear stress during the startup first increases, then it steeply drops, indicating sudden slip. Following this first drop, the stress increases again toward the steady state (which is actually not reached after 35 strain units), with its signal being characterized by persistent oscillations with progressively decreasing amplitude. It should be emphasized that this type of oscillatory stress undershoot reported by Dao and Archer is very different from the gradual and smooth undershoot and eventual unambiguous steady state reported by Costanzo *et al.* [11] for polystyrene. Nevertheless, the clear example reported by Dao and Archer suggests that stick-slip could be the cause of (qualitatively different) undershoots.

In this work, we systematically investigate the possible role of slip at the wall in inducing a stress undershoot in transient shear by running multichain sliplink simulations that include slip at the wall. Indeed, simulations allow for more detailed observables than experiments do. To that purpose, we modified the well-established primitive chain network (PCN) simulation code by introducing parallel solid plates confining a slab of bulk polymers and by grafting other polymers at the wall. In the simulation, one of the plates starts moving with a constant velocity, thus generating a shear flow. The plate motion propagates to the bulk liquid, but a slip velocity is also introduced. The latter is determined by imposing that the shear stress is the same at the wall and in the bulk. Similar to the earlier studies [26–29] mentioned above, for the effect of slippage on the viscosity, here we examine the stress response during the entire transient shearing from the start of the flow up to the steady state. Simulations are run for different values of shear rate, bulk chain molar mass, and grafted-chain density and molar mass. Effects of the simulation box thickness are also examined.

## II. MODEL AND SIMULATIONS

The simulation code used here is the same as that employed in earlier studies of shear flows [7,18,30–34], augmented for the presence of parallel walls, at which slip can take place. In the simulation, the bulk entangled polymeric system is replaced by a network consisting of strands, nodes, and dangling ends. Each polymer chain corresponds to a path connecting dangling ends through strands and nodes. At each node, two polymer chains are connected by a sliplink through which the two chains are allowed to slide along their backbone, with the sliplink somehow restricting the lateral motion. Sliplinks are removed when a chain end goes through them by either reptation or fluctuation. Conversely, a new sliplink is created on the dangling end (by "hooking" a surrounding chain) when the dangling end itself is long enough. The state variables are the sliplink position $\{\mathbf{R}\}$, the number $\{n\}$ of Kuhn segments in each strand and in the dangling ends, and the number $\{Z\}$ of strands (including dangling ends) in each chain. The sliplink positions $\{\mathbf{R}\}$ obey a Langevin-type equation of motion, i.e., a force balance involving the drag force, the strand tensions, an osmotic force, and a random one. As is usual in Brownian simulations, no other interchain forces are included. A force balance also controls the rate of change of $\{n\}$, describing chain sliding through sliplinks. Units of length, energy, and time are the average strand length $a$ at equilibrium, the thermal energy $kT$, and the diffusion time of the node $\tau = \zeta a^2/6kT$, with $\zeta$ being the friction coefficient of the node (resulting from the four half-strands emanating from it). We also normalize $\{n\}$ by taking the ratio to its average equilibrium value $n_0$.

In nondimensional units, the equation of change of the sliplink position $\{\mathbf{R}\}$ is written as

$$\dot{\mathbf{R}} - \mathbf{k}\cdot\mathbf{R} = \frac{1}{2}\sum_{i=1}^{4}\frac{\mathbf{r}_i}{n_i} - \frac{1}{3}\nabla\mu + \mathbf{F}. \tag{1}$$

Here, $\mathbf{k}$ is the velocity gradient tensor, $\mathbf{r}_i$ is the $i$th strand vector emanating from the sliplink, and hence, the sum is the result of the four elastic Gaussian forces acting on the sliplink. The chemical potential $\mu$, introduced to control density fluctuations, is derived from the following free energy expression:

$$J = \begin{cases} \varepsilon\left(\dfrac{\phi(\mathbf{R})}{\langle\phi\rangle} - 1\right)^2 & \text{for } \phi(\mathbf{R}) > \langle\phi\rangle, \\ 0 & \text{for } \phi(\mathbf{R}) \le \langle\phi\rangle. \end{cases} \tag{2}$$

Here, $\phi(\mathbf{R})$ is the local strand density, $\langle\phi\rangle$ is its average value in the simulation box, and $\varepsilon$ (fixed at 0.5) is the compressibility. In Eq. (1), $\mathbf{F}$ is the Gaussian random force obeying $\langle\mathbf{F}\rangle = \mathbf{0}$ and $\langle\mathbf{F}(t)\mathbf{F}(t')\rangle = 2\delta(t-t')\boldsymbol{I}$.

The time evolution of $\{n\}$ is similarly written as

$$\frac{\dot{n}}{\varphi} = \left(\frac{r_i}{n_i} - \frac{r_{i-1}}{n_{i-1}}\right) - \frac{1}{3}\nabla\mu + f. \tag{3}$$

Here, $\dot{n}$ is the rate of change of $n$ in the $i$th strand due to monomer sliding from/to the $(i-1)$th strand and $\varphi$ is the average local linear monomer density defined as

$$\varphi = \frac{1}{2}\left(\frac{n_i}{r_i} + \frac{n_{i-1}}{r_{i-1}}\right), \tag{4}$$

with $r$ being the strand length. The 1D random force $f$ obeys $\langle f\rangle = 0$ and $\langle f(t)f(t')\rangle = (2/3)\delta(t-t')$. Equations similar to

Eqs. (3) and (4) are used for the transfer of monomers from/to the $(i+1)$th strand.

Creation and destruction of entanglements at the chain ends are triggered by the value of $n$ in the dangling strands. If $n < 0.5$, the sliplink next to the dangling strand is removed. Vice versa, if $n > 1.5$, a new sliplink is created by randomly hooking another neighboring strand.

The bulk stress tensor is calculated from the tension in all strands of the simulation box as

$$\boldsymbol{\sigma} = \frac{3}{V}\sum_i \frac{\mathbf{r}_i \mathbf{r}_i}{n_i}, \tag{5}$$

where $V$ is the box volume. In previous studies for bulk polymers, periodic boundary conditions were used, and the flow was applied through a small affine deformation at each integration timestep. Simulations with this model reproduced linear and nonlinear rheology of entangled polymers semi-quantitatively [31–37].

In this study, we introduce wall boundary conditions to the cubic simulation box, as schematically represented in Fig. 1. To mimic confinement between parallel solid walls, we set reflective boundary conditions in the shear-gradient direction, while periodic boundary conditions are maintained in the shear and vorticity directions. Following earlier studies [38–41], we placed tethered polymers at the wall (i.e., with one grafted-chain end) with a grafting number density $\rho_g$ (number of anchored chains per unit area of the wall). Note that we did not include adhesion interactions between the solid wall and the polymers, just as we did not include intra-chain interactions other than entanglements. Possible dewetting phenomena are, therefore, not considered.

To simulate a shear flow, we adopted the procedure detailed below. We move the "upper" wall with a constant velocity $v_w$. Hence, the nominal shear rate $\dot{\gamma}_n$ is defined as $v_w/d$, where $d$ is the distance between the walls. In a real experiment, the motion propagates to the bulk via momentum transfer. However, in Brownian dynamics simulations of bulk polymers, momentum transfer in the shear-gradient direction is achieved by introducing (as mentioned above) a small affine shear deformation at each integration timestep, i.e., according to the magnitude of tensor $\mathbf{k}$ in Eq. (1). Because of slip, however, the magnitude of $\mathbf{k}$ (i.e., the bulk shear rate $\dot{\gamma}_b$) is not *a priori* known, except for the obvious inequality $\dot{\gamma}_b \leq \dot{\gamma}_n$. Here, we maintain the assumption that the shear rate $\dot{\gamma}_b$ is uniform throughout the bulk, i.e., that there is no banding.

Hence, by assuming that a same slip velocity $v_s$ is present at the upper and lower walls, the velocity field in the present simulation is given by (see Fig. 1)

$$v_x(y) = v_s + \dot{\gamma}_b y, \tag{6}$$

where the subscript $x$ stands for the shear direction, $y$ is the distance from the "lower" wall, and both the slip velocity $v_s$ and the bulk shear rate $\dot{\gamma}_b$ are *a priori* unknown. Because of the assumed symmetry, and since $v_x(d) = v_s + \dot{\gamma}_b d = v_w$, the two unknowns $v_s$ and $\dot{\gamma}_b$ are linked by the obvious relationship,

$$v_s = (v_w - \dot{\gamma}_b d)/2. \tag{7}$$

A second link between the two unknowns is provided by the condition that the shear stress at the wall $\sigma_w$ (generated by the tethered strands under the slip velocity $v_s$ and the bulk

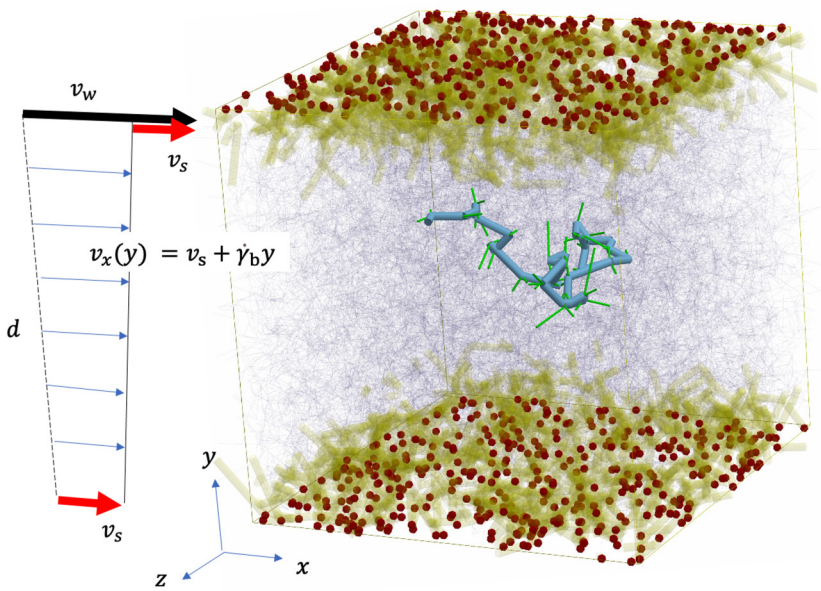


**FIG. 1.** Schematic representation of the simulation box with bulk chains shown by thin lines (in blue) and grafted ones by bold lines (in yellow). For better clarity, one of the bulk chains is highlighted, together with its entangled partner strands (in green). Dots (in red) on the walls indicate grafted-chain ends. For given values of all parameters, the bulk shear rate $\dot{\gamma}_b$ and the slip velocity $v_s$ are determined as detailed in the text. In this figure, the molecular weights of the bulk and grafted chains are $Z_b = 40$ and $Z_g = 5$, respectively, the grafting density is $\rho_g = 1$, and the box dimension is $d = 20$.

shear rate $\dot{\gamma}_b$) and that in the bulk $\sigma_b$ (generated by the bulk shear rate $\dot{\gamma}_b$) must be equal to one another,

$$\sigma_w = \sigma_b. \tag{8}$$

Here, $\sigma_b$ is calculated from Eq. (5), whereas $\sigma_w$ is given by

$$\sigma_w = \frac{3}{2A}\sum_i \frac{r_{ix}}{n_i}, \tag{9}$$

where $A = d^2$ is the interfacial area (the factor of 2 accounting for the fact that the sum is extended to the chains grafted to both the upper and lower plate) and $r_{ix}$ is the shear direction component of the strand vector.

At each simulation timestep, the two unknowns $v_s$ and $\dot{\gamma}_b$ are determined through the solution (by a numerical feedback) of Eqs. (7) and (8). Note, however, that such a solution does not always exist. Indeed, for sufficiently large values of either the grafted-chain density $\rho_g$ or of the grafted-chain length $Z_g$, the wall shear stress $\sigma_w$ is found to be larger than that $\sigma_b$ in the bulk, even if $v_s$ is set to zero. In the real world, under those conditions, slip at the wall is replaced by shear banding, with a layer of low shear rate close to the wall, and one of high shear rate in the bulk. Dealing with simulations accounting for shear banding is beyond the scope of this work. Work on shear banding is in progress by one of the authors of the present paper by using the dissipative particle dynamics (DPD) technique [42,43].

We performed simulations for several densities $\rho_g$ and molecular weights $Z_g$ of the grafted chains. Unless stated differently, the molecular weight $Z_b$ of the bulk polymers was fixed at 40, and the simulation box size $d$ at 20. Note that molecular masses are indicated in terms of the number of entangled strands at equilibrium, and the radius of gyration of the bulk chain at equilibrium is ca. 2.6, sufficiently smaller than the box size. Even under fast flows, when the bulk chain largest dimension grows up to 3.9, the latter remains sufficiently smaller than the box size $d$. For simplicity, both grafted and bulk chains are taken to be monodisperse. The viscoelastic longest relaxation time and the Rouse time for the bulk chains are obtained from the "classical" simulations (without walls), and they come out as $\tau_d = 5.5 \times 10^3$ and $\tau_R = 81$, respectively. For each parameter choice, eight independent simulations were run, starting from different initial configurations. After a sufficiently long equilibration, the motion of the upper wall was started. The nominal shear rate $\dot{\gamma}_n$ was varied from 0.001 to 0.3. This range corresponds to $5.5 \leq Wi \leq 1.6 \times 10^3$, and $8.1 \times 10^{-2} \leq Wi_R \leq 24$, which is very similar to the experimental range of Weissenberg numbers in the earlier study [11]. Flow-induced friction reduction [32,44] was ignored in this work.

## III. RESULTS AND DISCUSSION

Before showing steady shear results in the nonlinear range, it is convenient to report equilibrium results on grafted chains. Figure 2 shows the longest relaxation time $\tau_g$ of the grafted chains (entangled with the bulk chains having $Z_b = 40$) for several values of the grafted-chain density $\rho_g$ and molar mass $Z_g$. Such relaxation time was determined from the grafted-chain stress autocorrelation function. In Fig. 2(a), $\tau_g$ is shown to increase with increasing $Z_g$, as expected from the arm-retraction relaxation mechanism. In Fig. 2(b), $\tau_g$ is shown to decrease with increasing $\rho_g$, seemingly because short-lived entanglements between grafted chains increase, and correspondingly, the long-lived ones between bulk and grafted chains decrease (results not shown).

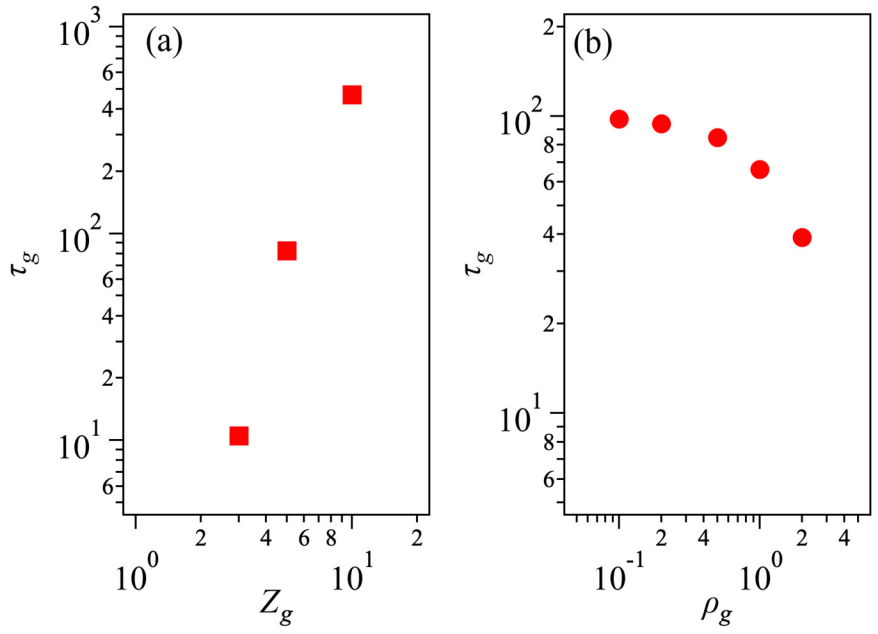


**FIG. 2.** Relaxation time $\tau_g$ of the grafted chains for the case $Z_b = 40$, as a function of $Z_g$ (a) and $\rho_g$ (b). Density $\rho_g$ is 0.5 in the left panel (a), and grafted-chain length $Z_g$ is 5 in the right one (b).

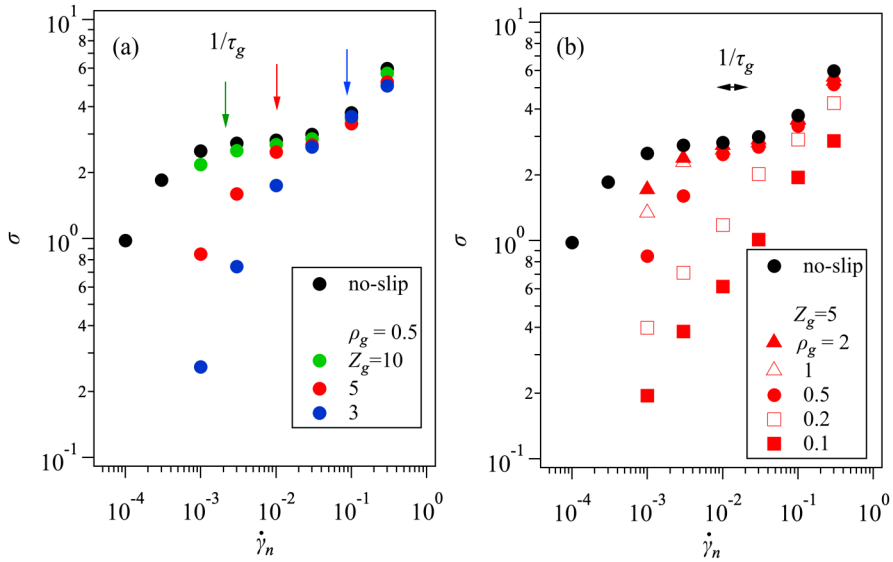


**FIG. 3.** Shear stress vs nominal shear rate for $Z_b = 40$. The left panel (a) is for $\rho_g = 0.5$ and various $Z_g$, while the right panel (b) is for $Z_g = 5$ and various $\rho_g$. Results for the no-slip case are also shown as black circles. Arrows indicate the relaxation rate $1/\tau_g$ of the grafted chains.

We now move on to show in Fig. 3 the steady-state shear stress $\sigma = \sigma_w = \sigma_b$ plotted against the nominal shear rate $\dot{\gamma}_n$, for several values of the grafted-chain molar mass $Z_g$ (left) and density $\rho_g$ (right), all for a bulk chain molar mass $Z_b = 40$. For comparison, the flow curve obtained from the bulk simulations without walls is also shown (black filled circles).

The arrows in Fig. 3(a) indicate the values of $1/\tau_g$ taken from panel (a) of Fig. 2. Hence, Fig. 3(a) shows that, at the fixed value $\rho_g = 0.5$, and for nominal shear rates $\dot{\gamma}_n$ larger than $1/\tau_g$, the shear stress (for all reported $Z_g$ values) essentially coincides with that of the simulations without walls. Conversely, when $\dot{\gamma}_n < 1/\tau_g$, the stress runs significantly below, revealing strong wall slip effects. In this low-shear-rate range, grafted chains have all the time to disentangle from the bulk ones, hence making bulk molecules free to slip away from the wall. We can call such behavior thermally induced slip. Actually, this low-shear-rate slip is an artifact because the model is forced to ignore the usual adhesion forces between the solid wall and bulk polymers. Inclusion of the adhesion forces would suppress the thermally induced slip.

The just described situation only applies at large enough grafted-chain densities. Indeed, Fig. 3(b) shows that, at the fixed value $Z_g = 5$, a large slip occurs also for $\dot{\gamma}_n > 1/\tau_g$ (the horizontal arrow showing the $1/\tau_g$ range 0.01–0.02), provided the density $\rho_g$ is sufficiently small. For $\dot{\gamma}_n > 1/\tau_g$, slip is no longer thermally induced, but rather it is due to convection (flow-induced slip). Such flow-induced slip is clearly visible in Fig. 3(b) at low grafted-chain densities.

We conclude the discussion of Fig. 3 by noting that, if larger values of $Z_g$ are considered (like $Z_g = 20$, or even $Z_g = 40$), the thermally induced slippage is suppressed in a sensible range of shear rates because $\tau_g$ becomes too large (results not shown). At the same time, however, also the flow-induced slippage is suppressed because the condition $\sigma_w = \sigma_b$ cannot be fulfilled, as mentioned in Sec. II. For such case, shear banding (instead of slip at the wall) prevails.

Figure 4 shows the slip velocity $v_s$ plotted against the nominal shear rate $\dot{\gamma}_n$. The straight line in both panels represents the maximum value of $v_s$, which is reached when $\dot{\gamma}_b = 0$, and it is given by $v_{s,\max} = \frac{1}{2} v_w = \frac{1}{2} \dot{\gamma}_n d = 10\dot{\gamma}_n$ [see Eq. (7)]. Before discussing Fig. 4, it is appropriate to recall the earlier experimental study of Durliat *et al.* [45] showing a slip transition at a critical shear rate, at which the value of $v_s$ abruptly increased by more than one decade. Both before and after such transition, the slip velocity grows linearly with the shear rate [45]. In our simulations, for sufficiently high values of $\rho_g$ and $Z_g$, the slip velocity $v_s$ steeply increases at values of $\dot{\gamma}_n$ somewhat smaller than 0.1 (see green circles in the left panel, and filled and unfilled triangles in the right one). Although the observed transition is not as sharp as experimentally reported, probably due to a size effect (our simulation "sample" is very thin), our results appear consistent with the experiments of Durliat *et al.* [45]. Moreover, after the transition, i.e., to the right of $\dot{\gamma}_n \approx 0.1$, our simulation results appear to approach a unit slope in Fig. 4, i.e., a linear dependence, consistently with Durliat *et al.* [45].

When the thermally induced slip dominates, i.e., at $\dot{\gamma}_n < 1/\tau_g$, the slip velocity $v_s$ runs very close to its maximum value, $v_{s,\max}$. This is apparent in the leftmost results in both panels of Fig. 4. Conversely, for $\dot{\gamma}_n > 1/\tau_g$, we observe the transition to flow-induced slip, where the slip velocity $v_s$ is significantly lower than $v_{s,\max}$. Such transition is particularly evident for $Z_g = 3$ and 5 in Fig. 4, whereas it falls too low to be observed for large values of either $\rho_g$ or $Z_g$. No transition at all is observed for low values of $\rho_g$ where, in spite of switching from the thermally induced to the flow-induced slippage, the slip velocity remains essentially coincident with $v_{s,\max}$ (see red squares in panel b). Indeed, at low densities, the grafted-chain stress is obviously very small, and hence, the equal value of stress in the bulk polymer implies a very small value of the bulk

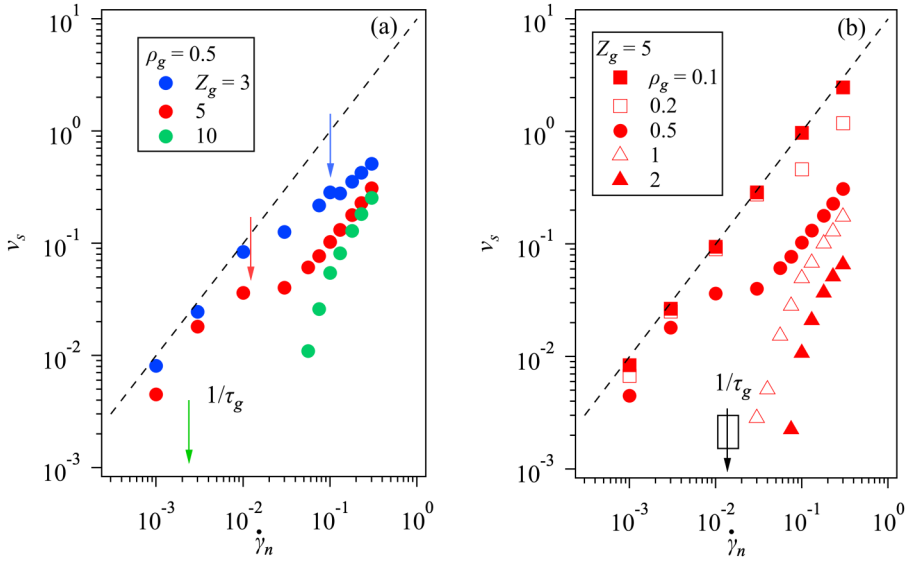


**FIG. 4.** Slip velocity $v_s$ against nominal shear rate for $Z_b = 40$. The left panel (a) is for $\rho_g = 0.5$, and several lengths $Z_g$ of the grafted chains, while the right one (b) is for $Z_g = 5$ and several $\rho_g$ values. The straight lines give the maximum possible value of $v_s$. Arrows indicate the relaxation rate 1/τg of the grafted chains.

shear rate $\dot{\gamma}_b$. For $\dot{\gamma}_b \approx 0$, from Eq. (3), we then get $v_s \approx \frac{1}{2} v_w = v_{s,\max}$.

Figure 5 shows the slip velocity $v_s$ as a function of the shear stress $\sigma$ for several $Z_g$ (left panel) and $\rho_g$ (middle panel) values. Panel (a) shows that, for any value of $\sigma$, the slip velocity increases with decreasing length $Z_g$ of the grafted chains (for a fixed value of the grafting density). This is because shorter grafted chains develop the same value of stress only if the shear rate is increased. An increasing shear rate then implies a higher value of the slip velocity (see Fig. 4). A similar argument can be used for panel (b), where it is apparent that, for a given $\sigma$, the slip velocity increases with decreasing grafting density (for a fixed grafted-chain length). In both panels, the slip velocity significantly increases with increasing the shear stress, beyond a critical value $\sigma_C$, which depends on $Z_g$ and $\rho_g$. As noted by Hatzikiriakos [46], the $v_s$ vs $\sigma$ curves superpose on each other if $v_s$ is plotted against $\sigma/\sigma_C$. In order to check the consistency of our results with the data of Hatzikiriakos, we determined $\sigma_C$ from the behavior at high $\sigma$ values (i.e., by

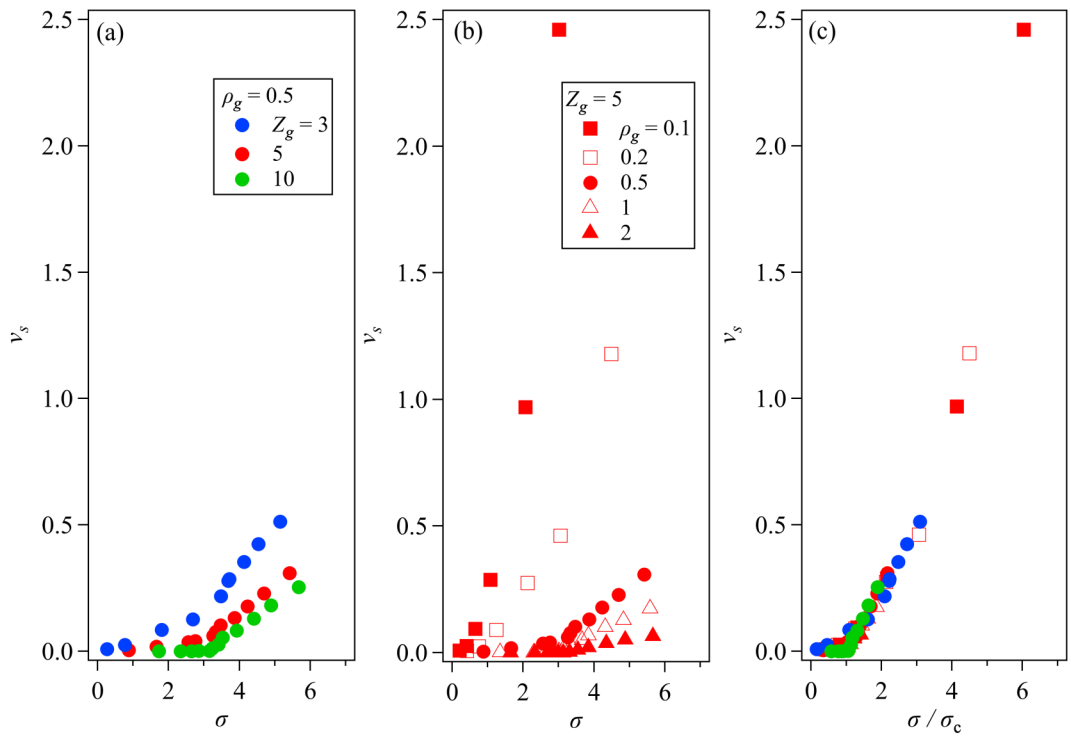


**FIG. 5.** Slip velocity $v_s$ against shear stress $\sigma$ for several $Z_g$ (left, a) and $\rho_g$ (middle, b) values. The right panel (c) shows $v_s$ plotted against the normalized shear stress $\sigma/\sigma_C$.

ignoring the data in the region of the artificial thermally induced slippage). Specifically, we estimated $\sigma_C$ in such a way that the normalized data superimpose for $\dot{\gamma}_n$ larger than $1/\tau_g$. For instance, for the case $Z_g = 3$ [blue circles in Fig. 5(a)], we determined $\sigma_C$ by ignoring results for $\sigma < 3$, where the slope is clearly different from that in the high $\sigma$ region insofar as results are still sensitive to thermally induced slippage. The overlap of our results for $\sigma > \sigma_C$ in Fig. 5(c) is consistent with the data of Hatzikiriakos [46].

The steady-state results we have shown so far (Figs. 3–5) indicate consistency of our simulations with the experimental data available in the literature for flow-induced slippage. We, therefore, proceed to examine the transient behavior in order to explore the possible role of slippage in creating the observed stress undershoot at high shear rates.

Figure 6 reports the viscosity growth curves for several $\rho_g$ and $Z_g$ values. Here, the "apparent" viscosity was calculated as $\eta_a = \sigma/\dot{\gamma}_n$. For comparison, the results from the no-slip simulations are also shown in Fig. 6 as broken curves. As previously shown in Fig. 2, Fig. 6 confirms that at low $\dot{\gamma}_n$ the stress (hence $\eta_a$) is lower than that in the no-slip case, due to the thermally induced slippage. At higher $\dot{\gamma}_n$, larger than the disengagement rate of the grafted chains shown in Fig. 3, the simulation results with and without slippage are close to one another (provided $\rho_g$ is large enough), as shown by way of example in Fig. 6(c). In these high-$\dot{\gamma}_n$ flows, the viscosity growth curve depends on $\rho_g$ and $Z_g$.

Panels from (a) to (c) in Fig. 6 show results at the fixed $Z_g = 5$ value, for three different values of $\rho_g$. As previously mentioned, the steady-state viscosity increases with increasing $\rho_g$ due to suppression of slippage. Concerning the

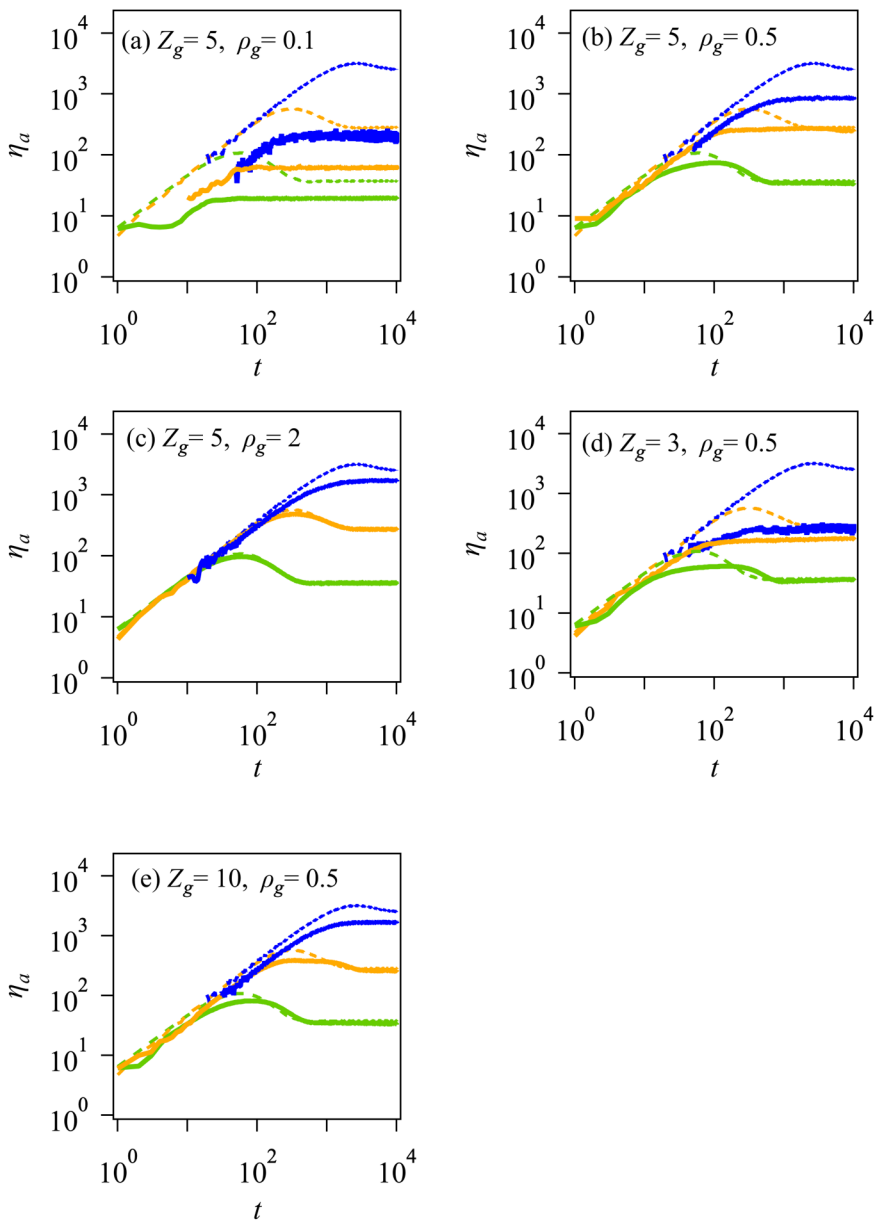


**FIG. 6.** Viscosity growth curves for several $\rho_g$ and $Z_g$ values. Nominal shear rates from top to bottom are 0.001 (blue),0.01 (orange), and 0.1 (green). Broken curves indicate results from the no-slip simulations.

transient behavior, the viscosity overshoot is reduced at low $\rho_g$ values. In fact, for $\rho_g = 0.1$ (panel a), there is no overshoot at all, except perhaps at the highest shear rate. For $\rho_g = 0.5$ (panel b), an overshoot is observed for $\dot{\gamma}_n \geq 0.03$, but the peak value is reduced, and its position is retarded, compared to the no-slip case. For $\rho_g = 2$, and at high rates, there is no difference between slip and no-slip simulations.

The effect of $Z_g$ can be seen in panels (b), (d), and (e) of Fig. 6, where $\rho_g$ is fixed at 0.5, while $Z_g$ takes the values 5, 3, and 10, respectively. These plots reveal that the slippage in slow flows is suppressed for large $Z_g$ because grafted chains remain entangled. Indeed, for $\dot{\gamma}_n < 0.01$, the steady-state viscosity decreases with decreasing $Z_g$, as already seen in Fig. 2. Conversely, in flows faster than the disengagement rate of grafted chains, the steady-state viscosity is almost independent of $Z_g$, and close to the no-slip value, because slippage does not occur. On the other hand, the transient behavior is somewhat sensitive to $Z_g$. By way of example, let us compare with one another the orange curves ($\dot{\gamma}_n = 0.01$) in panels (b), (d), and (e), where the overshoot appears very different. Namely, for $Z_g = 10$ (panel e), the overshoot is clearly visible, though the peak value is reduced, and the peak position is retarded, with respect to the no-slip case; for $Z_g = 5$ (panel b), the overshoot is sort of truncated; finally, for $Z_g = 3$ (panel d), the overshoot has completely disappeared.

Figure 7 shows further details of the transient behavior for $\dot{\gamma}_n = 0.03$ and $\rho_g = 0.5$, and for several $Z_g$ values. As mentioned above, the stress overshoot is reduced for short grafted chains [see Fig. 7(a)]. Transient values of the slip velocity $v_s$ are shown in Fig. 7(b). Here, $v_s$ first grows with time, and then, after a peak, it decreases toward the steady value. The time evolution of $v_s$ is similar to that of $\sigma$, as predicted by the stochastic model of Hatzikiriakos and Kalogerakis [29]. The decreasing branch of the $v_s$ and $\sigma$ curves moves to longer times as $Z_g$ decreases. This trend might seem counterintuitive in view of the fact that the relaxation time of the grafted chains decreases with decreasing $Z_g$. However, the delayed evolution of the stress with decreasing $Z_g$ is in fact due to the correspondingly smaller shear rate in the bulk, $\dot{\gamma}_b$. It is well known that in the shear startup of entangled polymers the orientation-induced stress peak is located at a shear deformation of ca. 2.3 [10], and at higher deformation values when also chain stretch comes into play ($Wi_R > 1$). The corresponding peak times are then obtained from the ratio of the peak shear deformation to the shear rate. The above is true, however, only when slip is absent. Conversely, when slip is present, the time at which such an effective deformation is reached, i.e., the peak time, becomes longer the smaller is $\dot{\gamma}_b$.

The number of entanglements formed at the interface between bulk and grafted chains, called $Z_{\text{int}}$, is shown in Fig. 7(c). $Z_{\text{int}}$ decreases with time from the equilibrium value due to the flow-induced disentanglement between bulk and grafted chains. At long times, the rates of creation and destruction of entanglements at the interface balance one another, and $Z_{\text{int}}$ reaches a steady value. Before reaching such a steady state, however, $Z_{\text{int}}$ shows a clear undershoot (see panel c). As expected, the position of the undershoot (i.e., the maximum disentanglement at the interface) coincides with that of the overshoot of $v_s$ and $\sigma$.

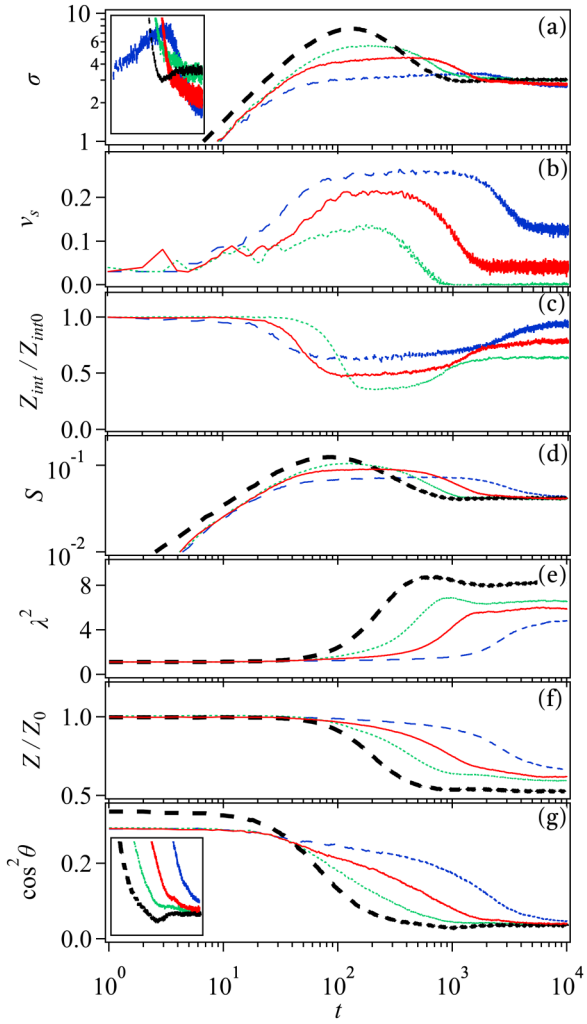


**FIG. 7.** Shear startup behavior at $\dot{\gamma}_n = 0.03$ ($Wi = 1.6 \times 10^2$ and $Wi_R = 2.4$) and $\rho_g = 0.5$ for $Z_g = 3$, 5, 10 (blue dashed, red solid, green dotted, respectively). (a) Shear stress, (b) slip velocity, (c) interfacial entanglement density, (d) strand orientation, (e) strand stretch, (f) bulk entanglement density, and (g) tilt angle. Dashed curves are from simulations without slip. Insets in panels (a) and (g) are magnified plots in the range $10^2 < t < 10^4$ to show undershoots in the no-slip case (thick black dashed curves).

In panels (d)–(f) of Fig. 7, the shear component $\sigma$ of the stress tensor of Eq. (5) is decomposed according to the decoupling approximation [5,7,18,32–34],

$$\sigma = \frac{3}{V}\sum_i \frac{r_{ix}r_{iy}}{n_i} = 3\upsilon\langle\frac{r_x r_y}{n}\rangle = 3\upsilon\langle\frac{r^2 u_x u_y}{n}\rangle$$
$$\approx 3\upsilon\langle\frac{r^2}{n}\rangle\langle u_x u_y\rangle = 3\langle\frac{Z}{Z_0}\rangle\lambda^2 S. \quad (10)$$

Here, $\upsilon = \langle Z/Z_0\rangle$ is the normalized strand density, $S = \langle u_x u_y\rangle$ is the strand orientation, and $\lambda^2 = \langle r^2/n\rangle$ is the square stretch ratio of the strand. Both with and without slippage, the stress overshoot is essentially determined by the strand orientation $S$ (panel d), whereas the strand stretch $\lambda^2$ comes into play after the overshoot (panel e), provided the Rouse-time-based Weissenberg number, $Wi_R$, is larger than unity. This is the case for the shear rate of 0.03 shown in Fig. 7 where $Wi_R = 2.4$. Flow-induced reduction of the

entanglement density $Z$ is also observed in panel f. For all quantities in Fig. 7, the curves are shifted to longer times with decreasing $Z_g$ due to the reduced shear rate in the bulk. Changes in the steady values are also consistent with change in the bulk shear rate.

Finally, panel (g) of Fig. 7 shows the effect of molecular tumbling through the average of $\cos^2\theta$, where $\theta$ is the tilt angle of the end-to-end vector of bulk chains to the shear direction. As reported previously [18], in the no-slip case $\cos^2\theta$ decreases over time and exhibits an undershoot before reaching the steady state. This undershoot reflects a coherent molecular tumbling at the startup of the shear flow, and it probably causes an undershoot of $\sigma$ (as assumed by Costanzo *et al.* [11] and confirmed by Nafar Sefiddashti *et al.* [17]), though very weak in panel (a) of Fig. 7. The undershoot of $\cos^2\theta$ is suppressed by the slippage due to the reduction of the bulk shear rate $\dot{\gamma}_b$. It so appears that slip mitigates molecular tumbling, presumably by inducing a stronger loss of coherence. Note also that in the present simulations with confining walls, the value of $\cos^2\theta$ at short times is smaller than that in simulations without walls because of the oriented chains near the surface.

Figure 8 shows a comparison among different bulk molecular weights $Z_b$ at a fixed shear rate of $\dot{\gamma}_n = 0.03$, and for $\rho_g = 0.5$ and $Z_g = 5$. At this rate, panel (a) shows that the steady state shear stress is insensitive to $Z_b$, as is typical of polymers in fast shear flows [47]. Also, the slip velocity $v_s$ (panel b) and the interfacial entanglement density $Z_{int}$ (panel c) do not vary much at the steady state. Conversely, as it is also typical [18], the transient responses are significantly affected by $Z_b$, with a significant increase of the overshoot with increasing molar mass. Here, however, in the presence of slip, we note that such an increase is more modest. Indeed, while the maximum value of the slip velocity $v_s$ increases significantly with increasing $Z_b$, the corresponding growth of the stress overshoot is minor. Hence, slippage reduces the magnitude of the overshoot with respect to the no-slippage case. Panel (c) also shows that the magnitude of the undershoot in the interfacial entanglement density $Z_{\text{int}}$ increases with increasing $Z_b$, and the recovering of $Z_{\text{int}}$ is retarded at large $Z_b$. This behavior of $v_s$ and $Z_{\text{int}}$ implies that the flow-induced slippage is enhanced for longer bulk chains. Notice, however, that no undershoot is observed in the $\sigma$ curves.

Finally, Fig. 9 shows the box-size effect, i.e., the effect of changing the thickness $d$ of the sheared layer on the same quantities of Fig. 8. However, the slip velocity is plotted here in the normalized form, i.e., as the sum of the upper and lower slip velocities divided by the wall velocity. Such a ratio, $r = 2v_s/v_w$, is appropriate because, for an equal value of $\dot{\gamma}_n$, changing $d$ proportionally increases $v_w$, and hence (albeit not necessarily by the same proportion) also $v_s$. It is also worth noting that, in view of Eq. (3), the above velocity ratio can also be written as $r = 1 - \dot{\gamma}_b/\dot{\gamma}_n$. The normalized slip velocity $r$ varies in the range 0–1, the lower limit implying a zero slip velocity, while the upper one a zero bulk shear rate (total slip).

Figure 9 shows that in the explored range, box-size effects are minor but non-negligible. This is because the slip velocity (as opposed to the normalized one) also plays a significant role. Indeed, by increasing the layer thickness $d$, the slip velocity also increases, and hence, grafted chains are dragged more effectively by the bulk flow; correspondingly, the shear stress somewhat increases (the green curve runs slightly higher in panel a). For the same reason, i.e., because of the increased slip velocity, the flow-induced disentanglement of the grafted chains from the bulk ones increases (the green curve runs slightly lower in panel c). In approaching the

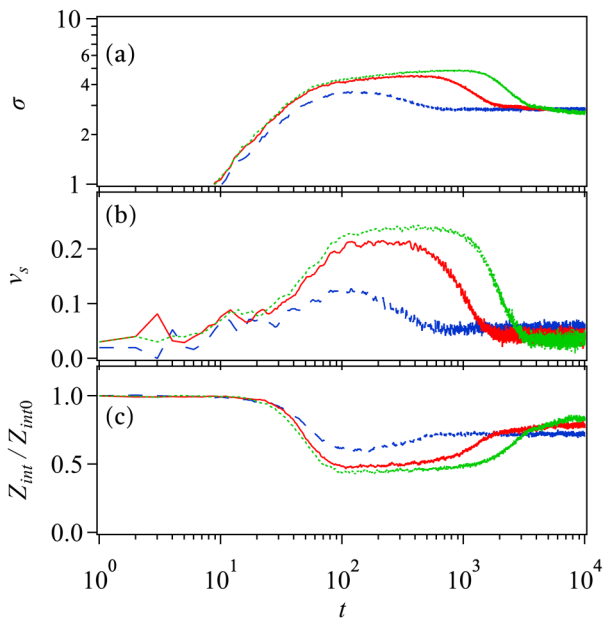


**FIG. 8.** Shear startup behavior of (a) shear stress, (b) slip velocity, and (c) interfacial entanglement density, for $Z_b = 20$ (blue dashed), 40 (red solid) and 60 (green dotted) with $\rho_g = 0.5$, $Z_g = 5$, and $\dot{\gamma}_n = 0.03$.

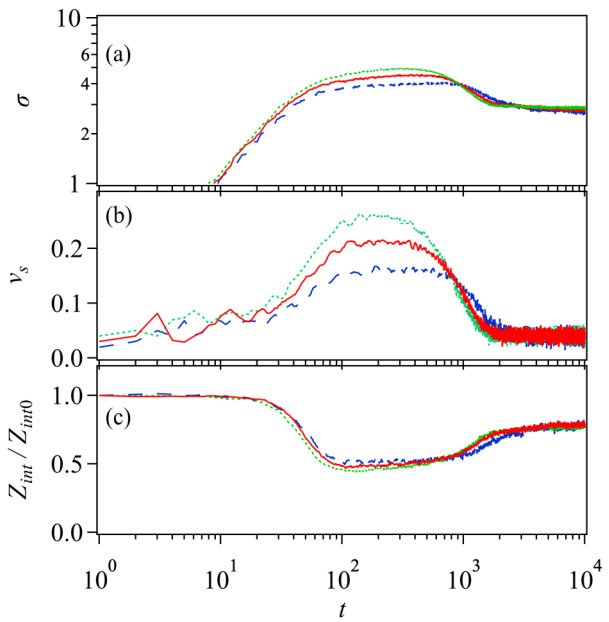


**FIG. 9.** Effect of changing the box size from $d = 15$ (blue dashed), to 20 (red solid), and 25 (green dotted) on shear startup at the fixed nominal shear rate $\dot{\gamma}_n = 0.03$. The observed quantities are (a) shear stress, (b) normalized slip velocity, and (c) interfacial entanglement density, all of them for $\rho_g = 0.5$, and $Z_g = 5$.

steady state, the ratio $v_s/v_w$ appears to decrease with increasing the layer thickness. In the limit of very large $d$ values (not explored here), we envisage that $\dot{\gamma}_b$ becomes very close to $\dot{\gamma}_n$, while $v_s$ approaches a nonzero value such that $\sigma_w$ remains equal to $\sigma_b$, the latter essentially determined by $\dot{\gamma}_n$.

Finally, concerning the main purpose of this work, i.e., investigating the role of wall slip in generating a stress undershoot in the shear startup, we observe that in the $\sigma$ plot of Fig. 9, as well as in all $\sigma$ plots of previous figures in the presence of slip, there is no sign of an undershoot.

## IV. CONCLUDING REMARKS

In this study, we extended the PCN model to deal with slippage between entangled polymeric liquids and solid walls with grafted polymers. We determined the slip velocity and the bulk shear rate by fulfilling the condition that the shear stress developed in the bulk chains and that resulting from the grafted chains must be equal to one another. By varying the molecular weight and the density of the grafted chains, we run several shear startup simulations. Results confirmed that, indeed, slip takes place if the chains attached at the wall are either short or sparsely grafted. For the transient startup behavior, the stress overshoot was found to be weakened by the slippage. During startup, the effect of slippage becomes more retarded when the grafted chains are longer. These results are consistent with earlier studies, and they essentially validate the model.

On the other hand, the main objective of this study, concerning the possible role of the wall slip in inducing a stress undershoot, was fully reached in the sense that no sign of undershoot was ever found in all simulations performed here. Disentanglement between grafted and bulk chains was found in our simulations in the stress overshoot region. However, such disentanglement did not induce any undershoot. On the contrary, it so appears that the slippage prevents the undershoot because it enhances the loss of coherence in the molecular tumbling.

We conclude by mentioning that the Brownian dynamics approach used here is not the only simulation technique able to investigate slip. The work based on the DPD method mentioned earlier [42,43] is now in progress by one of the authors.

## ACKNOWLEDGMENTS

Y.M. was supported, in part, by the Ogasawara Foundation, JST-CREST (No. JPMJCR1992), and NEDO (No. JPNP16010). D.V. and G.I. acknowledge support from EU through the ITN DODYNET project (Grant No. 765811).

## REFERENCES

[1] Bueche, F., and S. W. Harding, "New absolute molecular weight method for linear polymers," Rubber Chem. Technol. **32**(1), 99–106 (1959).

[2] Ferry, J. D., *Viscoelastic Properties of Polymers*, 3rd ed. (Wiley, New York, 1980).

[3] Graessley, W., *Polymeric Liquids & Networks: Dynamics and Rheology* (Garland Science, New York, 2008).

[4] Pearson, D., E. Herbolzheimer, N. Grizzuti, and G. Marrucci, "Transient behavior of entangled polymers at high shear rates," J. Polym. Sci. B Polym. Phys. **29**(13), 1589–1597 (1991).

[5] Pearson, D. S., A. D. Kiss, L. J. Fetters, and M. Doi, "Flow-induced birefringence of concentrated polyisoprene solutions," J. Rheol. **33**(3), 517–535 (1989).

[6] Osaki, K., T. Inoue, and T. Isomura, "Stress overshoot of polymer solutions at high rates of shear," J. Polym. Sci. B Polym. Phys. **38**(14), 1917–1925 (2000).

[7] Masubuchi, Y., and H. Watanabe, "Origin of stress overshoot under start-up shear in primitive chain network simulation," ACS Macro Lett. **3**(11), 1183–1186 (2014).

[8] Cao, J., and A. E. Likhtman, "Simulating startup shear of entangled polymer melts," ACS Macro Lett. **4**(12), 1376–1381 (2015).

[9] Masubuchi, Y., and H. Watanabe, "Stress-optical relationship in bead-spring simulations for entangled polymers under start-up shear flows," Nihon Reoroji Gakkaishi **44**(1), 65–68 (2016).

[10] Doi, M., and S. F. Edwards, *The Theory of Polymer Dynamics* (Clarendon, Oxford, 1986).

[11] Costanzo, S., Q. Huang, G. Ianniruberto, G. Marrucci, O. Hassager, and D. Vlassopoulos, "Shear and extensional rheology of polystyrene melts and solutions with the same number of entanglements," Macromolecules **49**(10), 3925–3935 (2016).

[12] Stephanou, P. S., T. Schweizer, and M. Kröger, "Communication: Appearance of undershoots in start-up shear: Experimental findings captured by tumbling-snake dynamics," J. Chem. Phys. **146**(16), 1–11 (2017).

[13] Auhl, D., J. Ramirez, A. E. Likhtman, P. Chambon, and C. Fernyhough, "Linear and nonlinear shear flow behavior of monodisperse polyisoprene melts with a large range of molecular weights," J. Rheol. **52**(3), 801–835 (2008).

[14] Nafar Sefiddashti, M. H., B. J. Edwards, and B. Khomami, "Elucidating the molecular rheology of entangled polymeric fluids via comparison of atomistic simulations and model predictions," Macromolecules **52**(21), 8124–8143 (2019).

[15] Nafar Sefiddashti, M. H., B. J. Edwards, and B. Khomami, "Individual chain dynamics of a polyethylene melt undergoing steady shear flow," J. Rheol. **59**(1), 119–153 (2015).

[16] Nafar Sefiddashti, M. H., B. J. Edwards, and B. Khomami, "Evaluation of reptation-based modeling of entangled polymeric fluids including chain rotation via nonequilibrium molecular dynamics simulation," Phys. Rev. Fluids **2**(8), 083301 (2017).

[17] Nafar Sefiddashti, M., B. Edwards, and B. Khomami, "Individual molecular dynamics of an entangled polyethylene melt undergoing steady shear flow: Steady-state and transient dynamics," Polymers **11**(3), 476 (2019).

[18] Masubuchi, Y., G. Ianniruberto, and G. Marrucci, "Stress undershoot of entangled polymers under fast startup shear flows in primitive chain network simulations," Nihon Reoroji Gakkaishi **46**(1), 23–28 (2018).

[19] Stephanou, P., and M. Kröger, "Assessment of the tumbling-snake model against linear and nonlinear rheological data of bidisperse polymer blends," Polymers **11**(2), 376 (2019).

[20] Hatzikiriakos, S. G., "Wall slip of molten polymers," Prog. Polym. Sci. **37**(4), 624–643 (2012).

[21] Denn, M. M., "Extrusion instabilities and wall slip," Annu. Rev. Fluid Mech. **33**(1), 265–287 (2001).

[22] Drda, P. P., and S. Q. Wang, "Stick-slip transition at polymer melt/solid interfaces," Phys. Rev. Lett. **75**(14), 2698–2701 (1995).

[23] Dao, T. T., and L. A. Archer, "Stick-slip dynamics of entangled polymer liquids," Langmuir **18**(7), 2616–2624 (2002).

[24] Migler, K. B., H. Hervet, and L. Leger, "Slip transition of a polymer melt under shear stress," Phys. Rev. Lett. **70**(3), 287–290 (1993).

[25] Brochard, F., and P. G. De Gennes, "Shear-dependent slippage at a polymer/solid interface," Langmuir **8**(12), 3033–3037 (1992).

[26] Pearson, J., and C. Petrie, On the melt-flow instability of extruded polymers, in *Polymer Systems: Deformation and Flow*, edited by R. Wetton and R. Whorlow (Macmillan, New York, 1965), pp. 163–187.

[27] Kazatchkov, I. B., and S. G. Hatzikiriakos, "Relaxation effects of slip in shear flow of linear molten polymers," Rheol. Acta **49**(3), 267–274 (2010).

[28] Ebrahimi, M., V. K. Konaganti, and S. G. Hatzikiriakos, "Dynamic slip of polydisperse linear polymers using partitioned plate," Phys. Fluids **30**(3), 030601 (2018).

[29] Hatzikiriakos, S. G., and N. Kalogerakis, "A dynamic slip velocity model for molten polymers based on a network kinetic theory," Rheol. Acta **33**(1), 38–47 (1994).

[30] Masubuchi, Y., J.-I. Takimoto, K. Koyama, G. Ianniruberto, G. Marrucci, and F. Greco, "Brownian simulations of a network of reptating primitive chains," J. Chem. Phys. **115**(9), 4387–4394 (2001).

[31] Masubuchi, Y., K. Furuichi, K. Horio, T. Uneyama, H. Watanabe, G. Ianniruberto, F. Greco, and G. Marrucci, "Primitive chain network simulations for entangled DNA solutions," J. Chem. Phys. **131**(11), 114906 (2009).

[32] Yaoita, T., T. Isaki, Y. Masubuchi, H. Watanabe, G. Ianniruberto, and G. Marrucci, "Primitive chain network simulation of elongational flows of entangled linear chains: Stretch/orientation-induced reduction of monomeric friction," Macromolecules **45**(6), 2773–2782 (2012).

[33] Masubuchi, Y., G. Ianniruberto, and G. Marrucci, "Primitive chain network simulations for H-polymers under fast shear," Soft Matter **16**(4), 1056–1065 (2020).

[34] Masubuchi, Y., Y. Doi, and T. Uneyama, "Primitive chain network simulations for the interrupted shear response of entangled polymeric liquids," Soft Matter **16**(28), 6654–6661 (2020).

[35] Masubuchi, Y., G. Ianniruberto, F. Greco, and G. Marrucci, "Entanglement molecular weight and frequency response of sliplink networks," J. Chem. Phys. **119**(13), 6925–6930 (2003).

[36] Masubuchi, Y., G. Ianniruberto, F. Greco, and G. Marrucci, "Molecular simulations of the long-time behaviour of entangled polymeric liquids by the primitive chain network model," Model. Simul. Mater. Sci. Eng. **12**(3), S91–S100 (2004).

[37] Masubuchi, Y., G. Ianniruberto, F. Greco, and G. Marrucci, "Quantitative comparison of primitive chain network simulations with literature data of linear viscoelasticity for polymer melts," J. Nonnewton. Fluid Mech. **149**(1–3), 87–92 (2008).

[38] Xu, F., M. M. Denn, and J. D. Schieber, "Stochastic chain simulation of wall slip in entangled polymer melts," J. Rheol. **51**(3), 451–464 (2007).

[39] Gay, C., "New concepts for the slippage of an entangled polymer melt at a grafted solid interface," Eur. Phys. J. B **7**(2), 251–262 (1999).

[40] Joshi, Y. M., A. K. Lele, and R. A. Mashelkar, "Molecular model for wall slip: Role of convective constraint release," Macromolecules **34**(10), 3412–3420 (2001).

[41] Kirk, J., M. Kröger, and P. Ilg, "Surface disentanglement and slip in a polymer melt: A molecular dynamics study," Macromolecules **51**(21), 8996–9010 (2018).

[42] Langeloth, M., Y. Masubuchi, M. C. Böhm, and F. Müller-plathe, "Recovering the reptation dynamics of polymer melts in dissipative particle dynamics simulations via slip-springs," J. Chem. Phys. **138**(2013), 104907 (2013).

[43] Masubuchi, Y., M. Langeloth, M. C. Böhm, T. Inoue, and F. Müller-Plathe, "A multichain slip-spring dissipative particle dynamics simulation method for entangled polymer solutions," Macromolecules **49**(23), 9186–9191 (2016).

[44] Ianniruberto, G., G. Marrucci, and Y. Masubuchi, "Melts of linear polymers in fast flows," Macromolecules **53**(13), 5023–5033 (2020).

[45] Durliat, E., H. Hervet, and L. Leger, "Influence of grafting density on wall slip of a polymer melt on a polymer brush," Europhys. Lett. **38**(5), 383–388 (1997).

[46] Hatzikiriakos, S. G., "A slip model for linear polymers based on adhesive failure," Int. Polym. Process. **8**(2), 135–142 (1993).

[47] Kulicke, W. M., and R. Kniewske, "The shear viscosity dependence on concentration, molecular weight, and shear rate of polystyrene solutions," Rheol. Acta **23**(1), 75–83 (1984).